The Role of Heteroatoms Leading to Hydrogen Bonds in View of Extended Chemical Stability of Organic Semiconductors

Christina Enengl, Sandra Enengl, Marek Havlicek, Philipp Stadler, Eric D. Glowacki, Markus C. Scharber, Matthew White, Kurt Hingerl, Eitan Ehrenfreund, Helmut Neugebauer, and Niyazi Serdar Sariciftci*

The major challenge in organic electronics concerns the stability of organic semiconductor materials which affects the operational lifetime of devices. Recent reports have shown that hydrogen-bonded pigments of the indigoid family are air- and moisture resistant. The magenta pigment quinacridone, a hydrogen-bonded molecule in the solid state with a pentacene like frame, is a perfect example for extraordinary chemical stability. Here, studies using in situ spectroscopic methods comparing quinacridone and pentacene are presented. A different spectral response of their radical cations is observed upon chemical doping. While in pentacene the barrier between doping and irreversible overoxidation is small, this stability toward overoxidation is increased by the heteroatomic structure, leading to hydrogen-bonded quinacridone. This work provides insight into molecular design principles that may lead to next-generation organic semiconductors with enhanced stability and performance.

1. Introduction

The development and synthesis of novel, high-performance organic semiconductors is of growing interest for future organic electronics. Herein, a lot of effort has been put in the functionalization of common molecular backbones, in order to enhance their chemical and physical properties. Such functionalized organic materials can be implemented in various applications with unique benefits due to their potential of low-cost processability, flexibility, stretchability, softness, and biocompatibility.[1–5]

Polyacenes and among them most prominently pentacene have extensively been studied for high-performance organic electronics.[6–9] By careful thin-film morphology control mobilities up to 3 $cm^2\ V^{-1}\ s^{-1}$ have been achieved in organic field-effect transistors (OFETs).[10] However, a detrimental aspect of pentacene is its affinity to rapid oxidation and related degradation that limits its lifetime and hence, its implementation into high-performance applications. Recent research has emphasized the derivatization of pentacene focusing on enhancing chemical stability.[11]

We took the view on one particular pigment, namely, quinacridone which is a promising candidate for the fabrication of electronic devices.[12–15] Earlier comparative studies are reported on OFET devices using quinacridone and pentacene thin films as active layers, respectively. Interestingly, respectable and comparable charge carrier mobilities are found.[16] However, differences are observed in the chemical stability of these active materials. While quinacridone is air-stable, pentacene is prone to rapid degradation. This behavior makes quinacridone curious in the field of organic devices, since this magenta pigment molecule adopts a pentacene backbone which is functionalized with adjacent asymmetric keto–amine groups leading to intermolecular hydrogen bonds in the solid state. Recently, Glowacki et al. reported quinacridone for ambipolar and biocompatible OFETs. Interestingly, the derivatization keeps the electronic assets of pentacene and concomitantly enhances chemical stability allowing operation under ambient and even aqueous conditions.[11,17,18] Furthermore, strong hydrogen bond interactions offer a new field for bio-inspired interfaces, its analogy to peptide groups enables bio-crafting in aqueous medium for sensor and detector applications.[19]

Not only pentacene like frame structures have awakened great interest in the last decades, also dyes and pigments in general which form intermolecular hydrogen bonds. Different studies on these compounds have been reported in the sense of improving stability as well as performance of thin-film organic devices.[20] Further promising candidates are diketopyrrolopyrroles showing enhanced charge transport and remarkable

C. Enengl, S. Enengl, Dr. M. Havlicek, Dr. P. Stadler, Dr. E. D. Glowacki, Dr. M. C. Scharber, Dr. M. White, Dr. H. Neugebauer, Prof. N. S. Sariciftci
Linz Institute for Organic Solar Cells (LIOS)
Physical Chemistry
Johannes Kepler University Linz
Altenbergerstraße 69, 4040 Linz, Austria
E-mail: Christina.Enengl@jku.at

Prof. K. Hingerl
Center for Surface and Nanoanalytics (ZONA)
Johannes Kepler University Linz
Altenbergerstraße 69, 4040 Linz, Austria

Prof. E. Ehrenfreund
Department of Physics and Solid State Institute
Technion-Israel Institute of Technology
Technion City, 32000 Haifa, Israel

DOI: 10.1002/adfm.201503241

thermal stability due to hydrogen-bonded crystal lattice.[21–23] Hence, materials having exactly these properties are likewise desirable for active materials in low-cost organic electronics.

In this work, we went beyond present device studies and elucidate profoundly the role of heteroatom functionalization which leads to hydrogen bonds in the solid state in view of its extraordinary chemical stability. Alternative derivatizations define stability mainly by resistance against oxidative attacks and, therefore, pursue to establish an electronic structure according to the stability window of oxygen and moisture, respectively. However, oxidative reactions are only one aspect. In view of extended operating lifetimes in devices self-degradation processes in these π-conjugated systems play an important role, too.

In particular cyclo-additions, dimerizations, as well as irreversible oxidation and reduction processes will deplete the active material upon long-term device operations. Therefore, our main interest has been elucidating the electronic and vibrational changes during doping and de-doping processes. Here, radical species are formed which we found to behave distinctively different in quinacridone as compared to pentacene. While in the latter the radical is reactive and prone to dimerize, say to self-degrade, this phenomenon is not observed in quinacridone which has secondary amines and carbonyl groups leading to intermolecular hydrogen bonds in the solid state. Exactly these phenomena are important properties for organic electronic applications and stimulated our detailed investigations.

In **Figure 1**, we see the schematic chemical structure of both molecules (a) pentacene and (b) quinacridone with hydrogen bonds in the solid state. In **Figure 2**, the corresponding reaction mechanism upon doping for both semiconductors is summarized. We emphasize on the reversibility and thus chemical stability of quinacridone's radical cation. While in pentacene a fraction of the radical species reacts irreversibly to its dimer, we find just reversible doping and de-doping in quinacridone. Thus, the pristine quinacridone molecule forms air and moisture-stable products, not reacting further to different—often unwanted—species. This fits to the outstanding chemical stability and reversibility reported earlier for quinacridone and gives a promising guideline for future molecular designs and high-performance, stable organic optoelectronic materials.[11]

Chemical doping with iodine as an oxidation agent creates charge carriers in both organic materials similar to those formed in OFET devices. In light of our study on the doped form, viz., the radical's stability we prefer iodine doping for establishing a high and persistent amount of mobile charge carriers. With this doping we intend to simulate p-type operation in a device. Similar studies have already been conducted for pentacene.[24] During the exposure to iodine vapor of the materials, spectroscopic measurements are recorded to track changes on the electronic as well as vibrational level. This technique is denoted further as an in situ experiment. Here, we present a spectroscopic survey from the UV–vis to mid-IR range including electron paramagnetic resonance (EPR) studies. Additionally, a theoretical part including symmetry operations and determination of vibrations is included. Our goal is to elaborate the effects of introducing heteroatom functionalization and its role to the related chemical stability and reversibility. While for pentacene we can rely on numerous spectroscopic studies handling the electronic and vibrational structure,[24–26] little is known for quinacridone. In this paper, we pursue in-depth spectral investigations for both organic semiconductors to understand the improvements by introducing secondary amines and carbonyl groups leading to hydrogen bonds in the solid state. Hence, we reveal useful information for quinacridone and also concomitantly new aspects for pentacene. This work elucidates from a spectroscopic point of view a molecular design principle for next-generation organic semiconductors with enhanced stability, lifetime and performance.

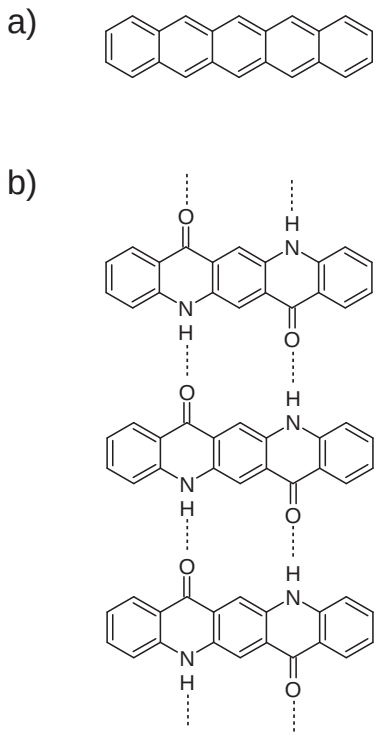

Figure 1. Schematic chemical structure of a) pentacene and b) quinacridone with intermolecular hydrogen bonds in the solid state.

2. Results and Discussion

2.1. Charge Carriers Obtained by Chemical Doping

By means of chemical doping (introducing p-type mobile charge carriers) the electrical conductivity of intrinsic molecular semiconductors can be increased by orders of magnitudes. In case of pentacene[25,27] as well as quinacridone we achieve a rise of the conductivity. **Figure 3** shows the change of electrical conductivity of thin-films of (a) pentacene and (b) quinacridone during exposure to iodine vapor for 1 h at room temperature. Both as-deposited films behave like an intrinsic semiconductor. After exposure to iodine vapor the conductivity reaches 70 S cm^{-1} for pentacene and 1.6×10^{-4} S cm^{-1} for quinacridone, respectively. In the case of doped pentacene, Minakata et al. reported similar values up to 100 S cm^{-1}.[25,27] The conductivity of doped quinacridone is more than four orders of magnitude lower than for pentacene.

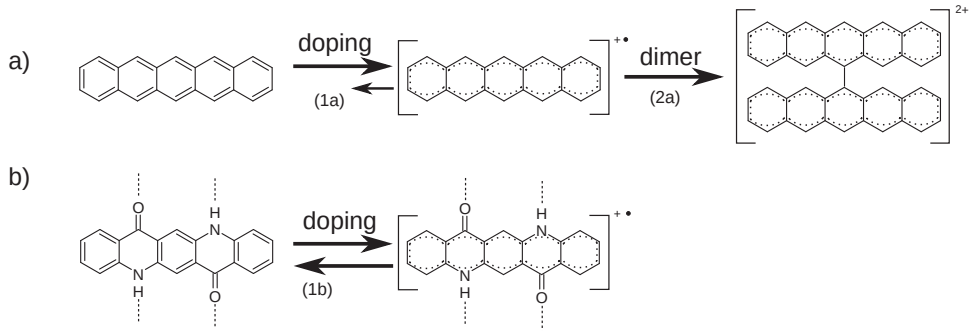

Figure 2. We see the proposed reaction mechanism of a) pentacene and b) quinacridone. Pentacene forms during oxidation a radical cation which is reacting further irreversibly to a dimeric species. In contrast, with quinacridone the formation of the radical cation is a reversible process.

However, these results prove the existence of moveable charge carriers for both molecular systems. In addition, comparative mobility studies in OFET devices have been carried out for both semiconducting materials showing similar values.[16] The mobility for pentacene is in the range of 0.1–1 $cm^2\ V^{-1}\ s^{-1}$ while quinacridone shows comparable mobilities, around 0.1 $cm^2\ V^{-1}\ s^{-1}$ using the same device preparation techniques.[16] Hence, we can calculate the number of free charge carriers for these materials. While in the case of pentacene we obtain 4×10^{20}–$4 \times 10^{21}\ cm^{-3}$, quinacridone has around $10^{16}\ cm^{-3}$ which is by a factor of 10^4–10^5 smaller. This calculation indicates that oxidation with iodine creates a smaller amount of charge carriers in quinacridone as compared to pentacene.

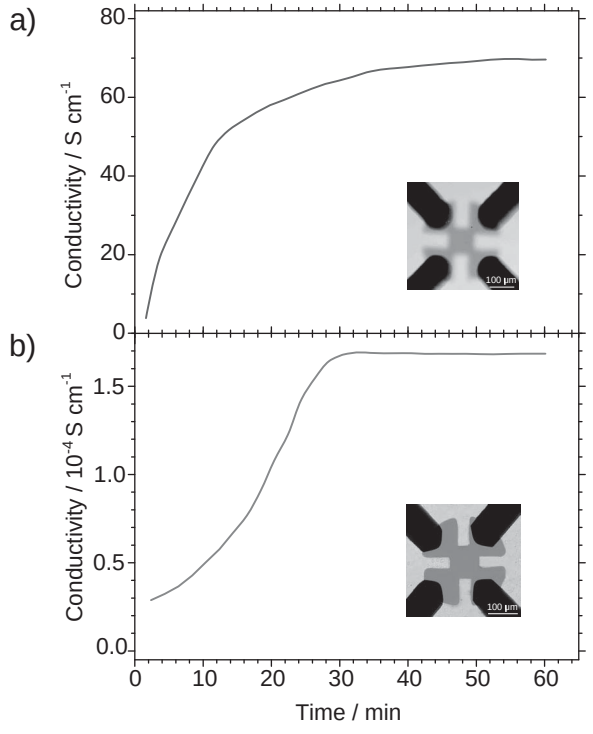

Figure 3. Electrical conductivity of a) pentacene and b) quinacridone film with iodine doping for 1 h at room temperature. During doping the conductivity increases up to 70 S cm^{-1} for pentacene and 1.6×10^{-4} S cm^{-1} for quinacridone, respectively. The inset shows the image of the van der Pauw sample geometry.

This difference in conductivity is explained by a distinct number of free charge carriers in pentacene and quinacridone. The smaller amount of charge carriers in quinacridone indicates an enhanced chemical stability against oxidative attacks. In addition, we use density functional theory (DFT) calculations for proving lower reactivity against oxygen and other oxidizing agents due to the deeper highest occupied molecular orbital (HOMO) level of quinacridone which we obtain as a result. In **Figure 4**, we see the calculated frontier orbitals and their relative energy levels from DFT calculations in the pristine form, in agreement with previous calculations.[11] We observe similar lowest unoccupied molecular orbital (LUMO) levels for pentacene and the hydrogen-bonded analog quinacridone. Differences are observed in the HOMO levels. Quinacridone results in a more stable HOMO level as compared to pentacene due to incorporation of heteroatoms. This deeper HOMO level of quinacridone correlates with better air stability. The calculated HOMO–LUMO gaps for both semiconductors are different from experimental data, since these molecules are considered in vacuum. Thus, functional groups such as carbonyl and secondary amines in quinacridone which enforce intermolecular hydrogen bonds in the solid state are the key issue for chemical stability in this type of compounds.

2.2. Symmetry Operations and Determination of Vibrations

Before coming to the spectroscopic characterization of the charge carriers we assign the peaks from the IR and Raman spectra to corresponding vibrations of these molecules for understanding the spectral changes upon doping.

In **Figure 5**, we see the schematic chemical structure of pentacene and quinacridone with their symmetry operations. Although both molecules have the same number of atoms, they differ in the number of symmetry operations due to the fact that pentacene does not contain secondary amines and carbonyl groups. Hence, pentacene has a higher symmetry.

A single pentacene molecule has D_{2h} as the point group and 102 normal modes. Following the procedure by Harris et al.,[28] these vibrational modes are divided into

$$\Gamma_{vib} = 18A_g + 17B_{1g} + 7B_{2g} + 9B_{3g} + 8A_u + 9B_{1u} + 17B_{2u} + 17B_{3u} \quad (1)$$

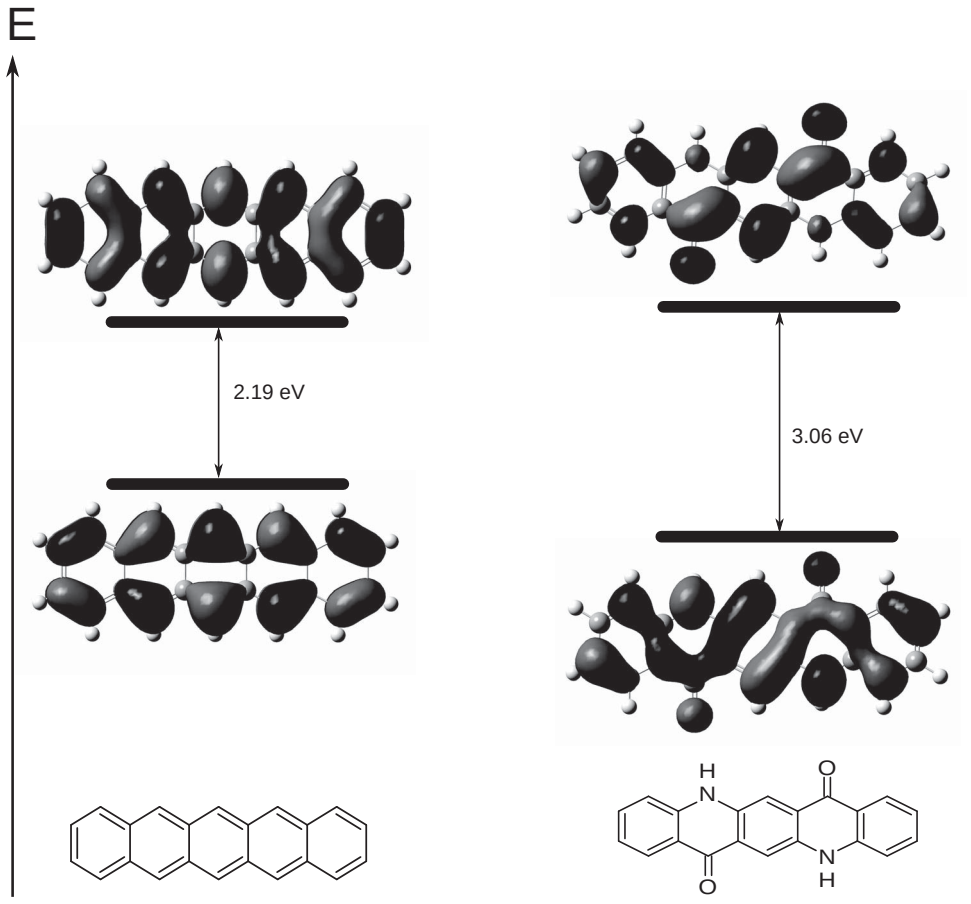

Figure 4. Calculated frontier orbitals for pentacene and quinacridone and their relative energy levels from DFT calculations in the pristine form. Similar LUMO levels for pentacene and the hydrogen-bonded analog quinacridone are obtained from calculations while quinacridone results in a more stable HOMO level as compared to pentacene.

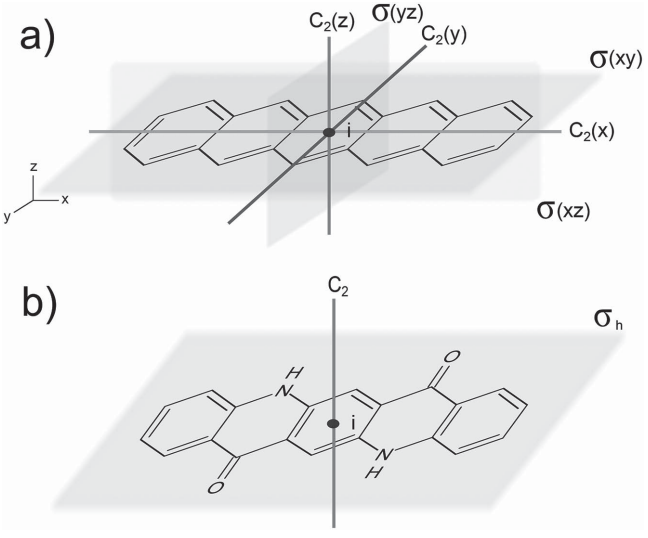

Figure 5. Schematic chemical structure of a) pentacene and b) quinacridone with their symmetry operations. Pentacene has eight symmetry operations, namely, E, $C_2(x)$, $C_2(y)$, $C_2(z)$, i, $\sigma(xy)$, $\sigma(xz)$, $\sigma(yz)$ and quinacridone has four symmetry operations E, C_2, i, σ_h. E: identity, C_2: twofold rotation axis, i: inversion, σ: mirror plane, and σ_h: horizontal mirror plane.

The difference between the Mulliken symbols A and B is the character under the principal rotational operation which is +1 for A and −1 for B. The subscripts g and u, standing for gerade and ungerade, respectively, represent the symmetry with respect to inversion.[28] Compared to the molecule quinacridone, which belongs to the point group C_{2h}, quinacridone also has 102 normal modes. Its vibrational modes are

$$\Gamma_{vib} = 35A_g + 16B_g + 17A_u + 34B_u \quad (2)$$

Since both molecules have an inversion center, the selection rules are such that the rule of mutual exclusion holds. Thus, gerade vibrations are Raman-active, whereas ungerade modes are IR-active only. For pentacene the vibrational modes assigned to A_u are silent modes.

In **Figure 6**, we see the Raman spectrum (top) of the pristine powder of (a) pentacene and (b) quinacridone as well as the attenuated total reflection Fourier-transform infrared (ATR-FTIR) spectrum (bottom) of these compounds in a thin-film deposited on a ZnSe crystal. Characteristic Raman bands for the secondary amines and carbonyl groups of quinacridone (Figure 6b, top) are assigned to 1516 and 1651 cm^{-1}, respectively. In the IR spectrum (Figure 6b, bottom), the broad band between 2900 and 3400 cm^{-1} indicates the hydrogen bonds

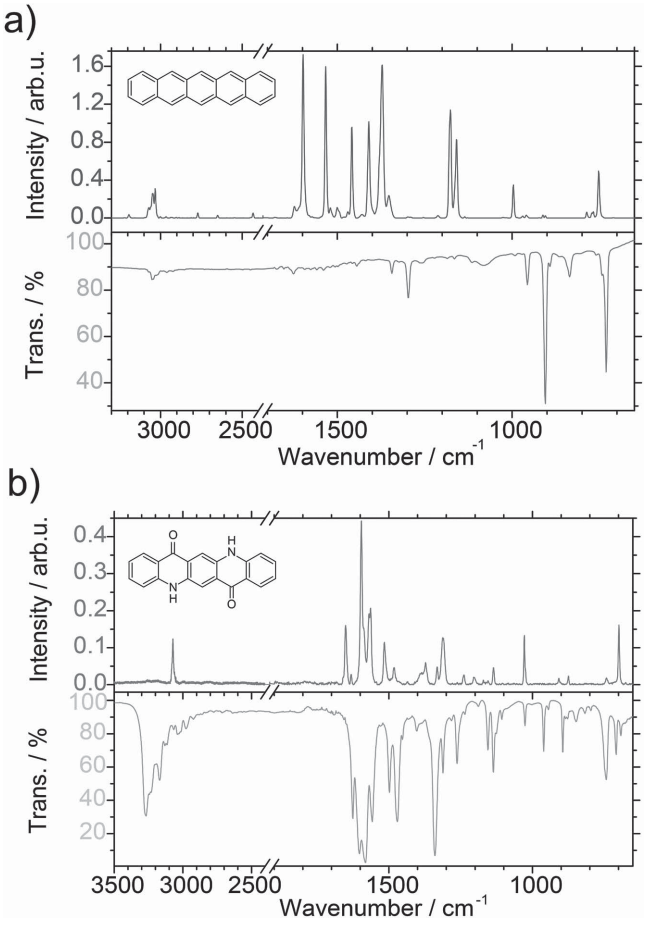

Figure 6. Raman spectra (top) of pristine powder and ATR-FTIR spectra (bottom, plotted in transmittance) as a thin-film of a) pentacene and b) quinacridone.

between neighboring quinacridone molecules. Similar results are observed for different compounds, also forming intermolecular hydrogen bonds.[29] The strong peaks on top of the broad hydrogen band indicate other vibrations of quinacridone, for instance, the N—H stretching vibration at 3267 cm^{-1}. The N—H deformation vibrations are visible at 1603, 1582, and 1558 cm^{-1}. At 1625 cm^{-1} we observe a strong peak for C=O vibration. We determined other main characteristic Raman and IR peaks of pentacene and quinacridone with the help of the Gaussian 09 program[30] and they are listed in Tables S1 and S2 (Supporting Information), respectively.

2.3. Spectroscopic Characterization of Charge Carriers from UV–Vis to Mid-IR

As next step in situ spectroscopic characterizations resolve the qualitative changes in view of chemical stability and lifetime. In **Figure 7**a, we depict two graphs showing the absorption spectra (UV–vis–near-IR) of pristine pentacene (black lines) and pentacene upon oxidation for 60 min. Most significant changes are seen in pentacene after the first few minutes. Immediately after initiating oxidation a broad band develops in the range of 350–600 nm (3.54–2.07 eV). These results have been confirmed in literature.[25,26] Brinkmann et al. and references therein[25,31] attributed the peak at 500 nm (2.48 eV) to molecular iodine and the new bands at about 400 nm (3.1 eV) to polyiodide ions, such as I_3^- and I_5^-. Concerning chemical stability we have now been interested to crosscheck also small changes occurring in the long run for 1 h. An interesting pentacene-related effect is observed in the second plot of Figure 7a. Here, an intense peak at 1010 nm (1.23 eV) appears right after the oxidation starts and stays nearly the same after 45 min while after 45 min a peak at 900 nm (1.38 eV) starts to arise, indicating that the oxidized species reacts further. The increase at 1100 nm (1.13 eV) describes the onset of a peak in the mid-IR and will be discussed there. We interpret these changes occurring over time as instability of the pentacene's oxidized species which are reacting further to its dimer "$(pentacene)^{2+}_2$" indicated as reaction (2a) in Figure 2. In Figure 7b, we illustrate the corresponding absorption spectra of the pristine film of quinacridone (black line) and quinacridone upon doping for 60 min. The spectrum of quinacridone does not reveal the strong changes as in the pentacene case (Figure 7a). Only very small changes in the range of 350–550 nm (3.54–2.25 eV) are visible. Due to the strong chemical stability, consistent with DFT calculations, quinacridone is oxidized in a much lower degree. Further, it forms stable radical cations, since effects over long-term measurements for about 1 h have not been detected (reaction (1b) in Figure 2).

We now turn to the changes tracked in the mid-IR range. In **Figure 8**, we present the difference spectra (reference spectrum is the pristine thin film of the semiconductors, respectively) in the IR range from 1600 to 7000 cm^{-1} (0.2 to 0.87 eV) for (a) pentacene and (b) quinacridone and from 650 to 1700 cm^{-1} (0.08 to 0.21 eV) for (c) pentacene and (d) quinacridone recorded at the same conditions as in UV–vis measurements. For pentacene (Figure 8a) two broad absorption bands develop initially simultaneously at 6900 cm^{-1} (0.86 eV) and 1700 cm^{-1} (0.21 eV) as indicated in reaction (1a) in Figure 2. The band at 6900 cm^{-1} (0.86 eV) is the continuation of the onset at 1100 nm (1.13 eV), mentioned already in the UV–vis–near-IR part. At the beginning of the oxidation process the absorption band at lower energy increases faster as compared to the band at 6900 cm^{-1} (0.86 eV). Again we detect the dimerization effect after 40 min exposure time giving rise to reaction (2a) in Figure 2. The absorption band at higher energy undergoes a red shift and reaches a maximum at 6600 cm^{-1} (0.82 eV). During this shift of the broad band at higher energy, the absorption at 1700 cm^{-1} (0.21 eV) decreases. This behavior indicates that—as the oxidation of pentacene starts—a persistent dimerization occurs, leading to a loss of pentacene radical cations. In contrast, with quinacridone we do not observe any hints for further reactions, like dimerizations. In Figure 8b, we see a broad absorption band occurring at around 2700 cm^{-1} (0.33 eV) during the oxidation process (reaction (1b) in Figure 2). The negative bands in the region of 2920–3270 cm^{-1} (0.36–0.41 eV) are connected to the loss of absorption of the vibrations of ν CH_{arom} and ν NH, indicating that the molecular structure changes upon doping. However, here the behavior of the broad absorption band is reversible. It disappears by removing the iodine vapor and appears again by re-exposing the sample (Figure S1, Supporting Information).

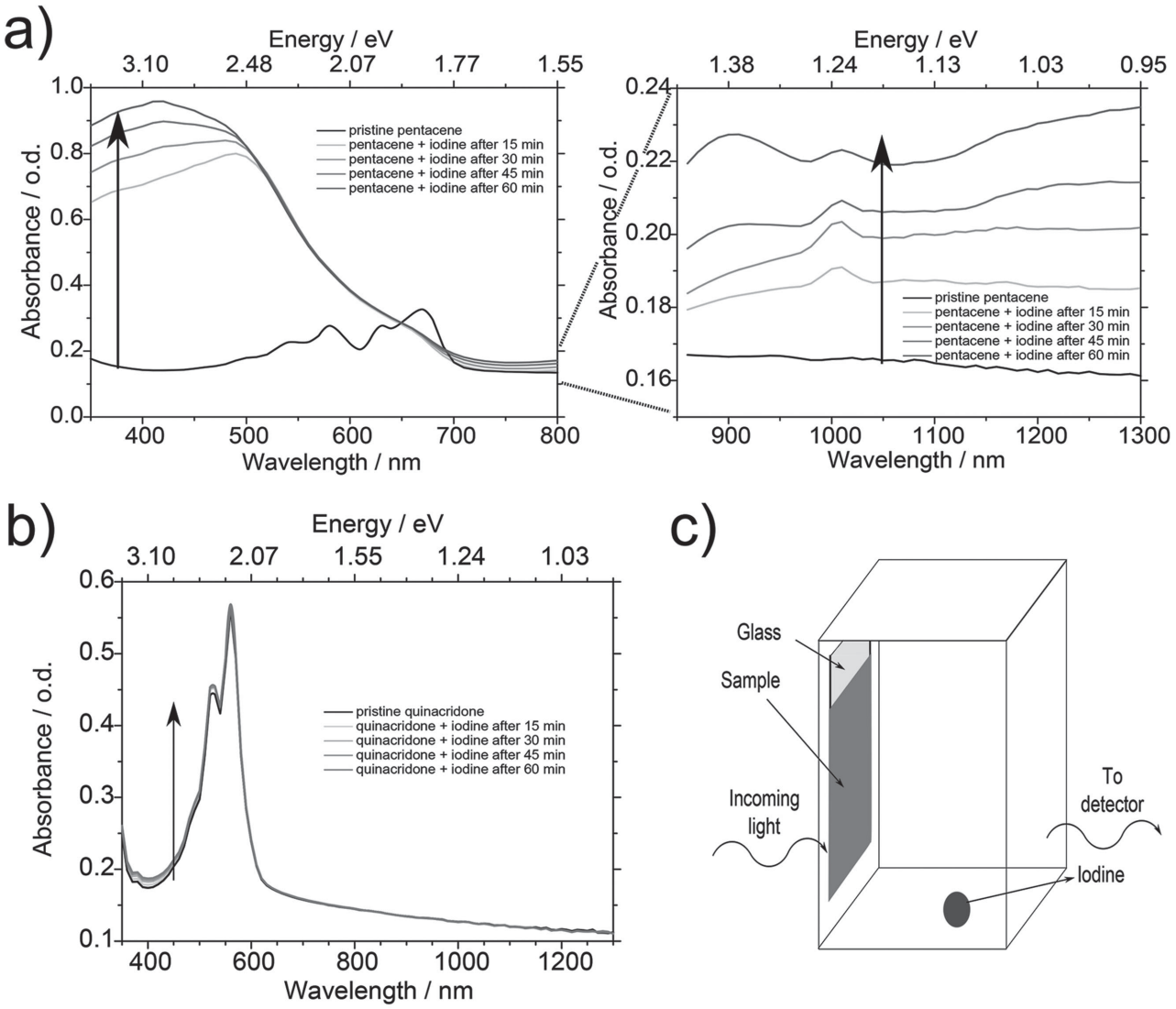

Figure 7. Absorption spectra of a pristine thin film (black line) of a) pentacene and b) quinacridone on glass. The colored lines represent the absorption spectra of pentacene and quinacridone exposed to iodine vapor for 60 min. New peaks at about 500 nm (2.48 eV), about 400 nm (3.1 eV), and bands at 900 and 1010 nm (1.38 and 1.23 eV) appear for pentacene while in the case of quinacridone only small changes in the range of 350–550 nm (3.54–2.25 eV) are visible. c) The schematic sketch of the transmittance chemical cell for in situ UV–vis measurements.

Such behavior cannot be reported for pentacene, pointing out the mentioned irreversibilities.

To understand how the charges are distributed on molecular level during the oxidation process, we take a closer look at the vibrational absorptions. Figure 8c,d shows the difference spectra in the IR range from 650 to 1700 cm^{-1} of pentacene and quinacridone, respectively. The reference spectrum is the pristine thin film of the organic molecules. In pentacene (Figure 8c), there are hardly any vibrations visible at the beginning of the oxidation process (reaction (1a) in Figure 2). This is a hint that the charge carriers are delocalized over the whole molecule. After 40 min iodine doping, we obtain new C=C and C—H vibrations in the region of 1150–1550 cm^{-1} explained by the dimerization of two "pentacene$^{+\bullet}$" radical cations to "(pentacene)$^{2+}{}_2$" (reaction (2a) in Figure 2). Quinacridone on the contrary behaves different. In Figure 8d, characteristic new peaks appear at 1623, 1573, and 1552 cm^{-1} which are assigned to new stretching vibrations like ν C=N and ν C=C. The N—H vibrations at 1603 and 1582 cm^{-1} disappear. Both vibrations have a B_u mode. Other appearing and disappearing peaks are assigned to C=C and C—H vibrations. Interestingly, all vibrations are strictly reversible. In Tables S1 and S2 (Supporting Information), the assignments of vibrations for pentacene and quinacridone are given in greater detail, respectively.

A reason for the strong appearing and disappearing peaks in quinacridone is that the charge carriers are probably more locked up in the cage of quinacridone as compared to pentacene. This can also be explained from calculated frontier orbitals of the pristine material (Figure 4), since the electron-rich part is close to the nitrogen atom. Thus, these calculations imply that the localization of the charge carriers are close to the

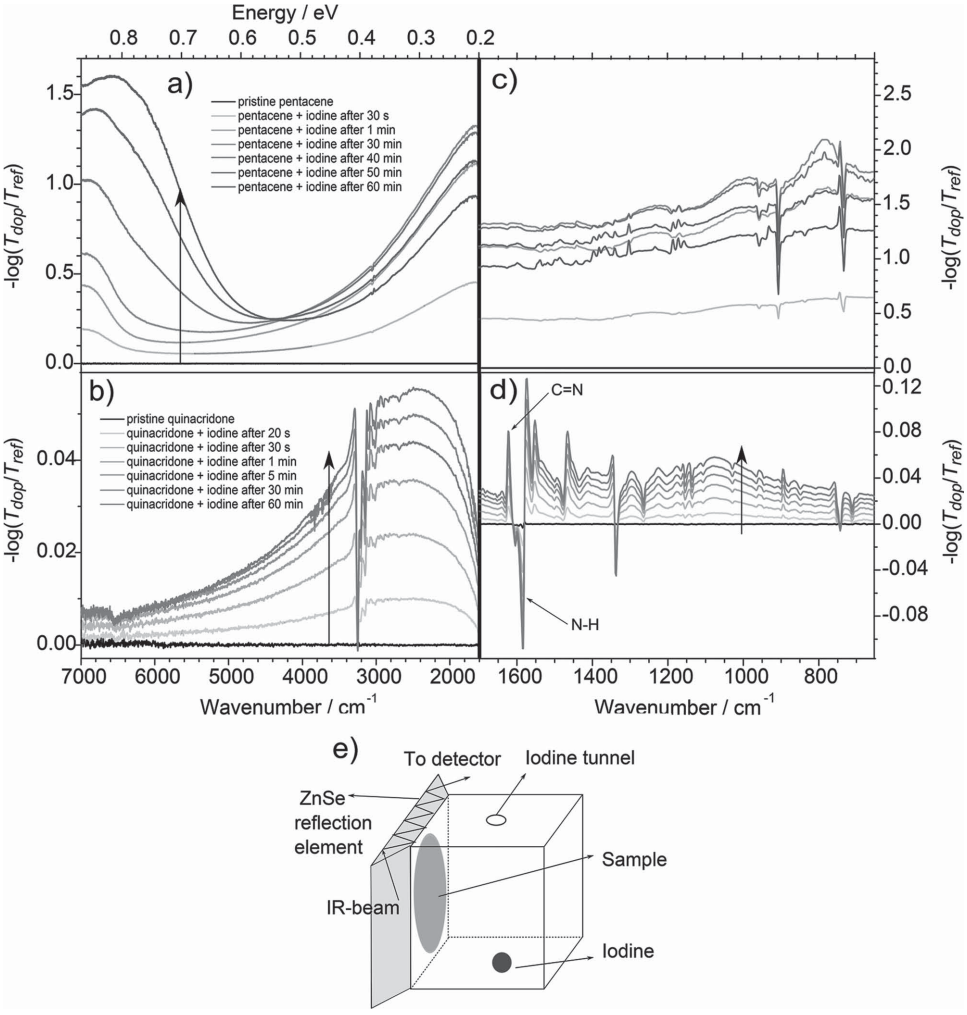

Figure 8. Difference spectra (reference spectrum is the pristine thin film of the semiconductors, respectively) in the IR range from 1600 to 7000 cm^{-1} (0.2 to 0.87 eV) for a) pentacene and b) quinacridone and the difference spectra in the range from 650 to 1700 cm^{-1} (0.08 to 0.21 eV) for c) pentacene and d) quinacridone which are recorded during the oxidation process for 60 min. a) In the case of pentacene two peaks at 6900 and 1700 cm^{-1} (0.86 and 0.21 eV) develop initially simultaneously while after 40 min of oxidation the absorption band at higher energy undergoes a red shift and reaches a maximum at 6600 cm^{-1} (0.82 eV). During this shift the band at 1700 cm^{-1} (0.21 eV) decreases. b) For quinacridone we observe a broad absorption band continuously increasing at 2700 cm^{-1} (0.33 eV). c) There are hardly any vibrational changes visible at the beginning of the oxidation process, while after 40 min iodine doping we obtain new C═C and C—H vibrations in the region of 1150–1550 cm^{-1}. d) For quinacridone characteristic new peaks appear at 1623, 1573, and 1552 cm^{-1}, which are assigned to new stretching vibrations like ν C═N and ν C═C. The N—H vibrations at 1603 and 1582 cm^{-1} disappear. e) The schematic sketch of the chemical cell for in situ IR measurements.

nitrogen atom, reflected in the experimental data by a strong stretching vibration of ν C═N at 1623 cm^{-1} for the radical cation "quinacridone$^{+\bullet}$". In contrast, with pentacene we observe a different situation, since no preferences are observed in the frontier orbital calculations for an electron. These results imply delocalization of the charge carriers over the whole molecule which is consistent with the spectroscopic data.

Although charge carriers in quinacridone are localized to its heteroatoms, both semiconductors show similar mobility values.[16] This is explained by different crystal structures of these molecules. While pentacene has a herringbone packing pattern with a π–π stacking distance between 5.9 and 7.5 Å,[32,33] quinacridone crystallizes in a brickwork-like structure, as linear hydrogen-bonded chains (about 2 Å) of molecules π–π upon one another (distance about 3.3 Å).[17] Due to transfer integral calculations, there is very little contribution for charge transport coming from hydrogen bond directions in quinacridone.[21] Additionally, these calculations show that closer π–π stacking distances correspond to higher mobility values.[21] Thus, the higher mobility in quinacridone due to closer π–π stacking is reduced by the localization of these charge carriers. Hence, both organic semiconductors result in similar charge carrier mobility values.

2.4. Characterization of Charge Carriers by EPR Measurements

A final insight to the radical stability is offered by in situ EPR measurements. The existence of "pentacene$^{+\bullet}$" and "quinacridone$^{+\bullet}$" and possible side reactions can be tracked using a time-dependent intensity analysis.

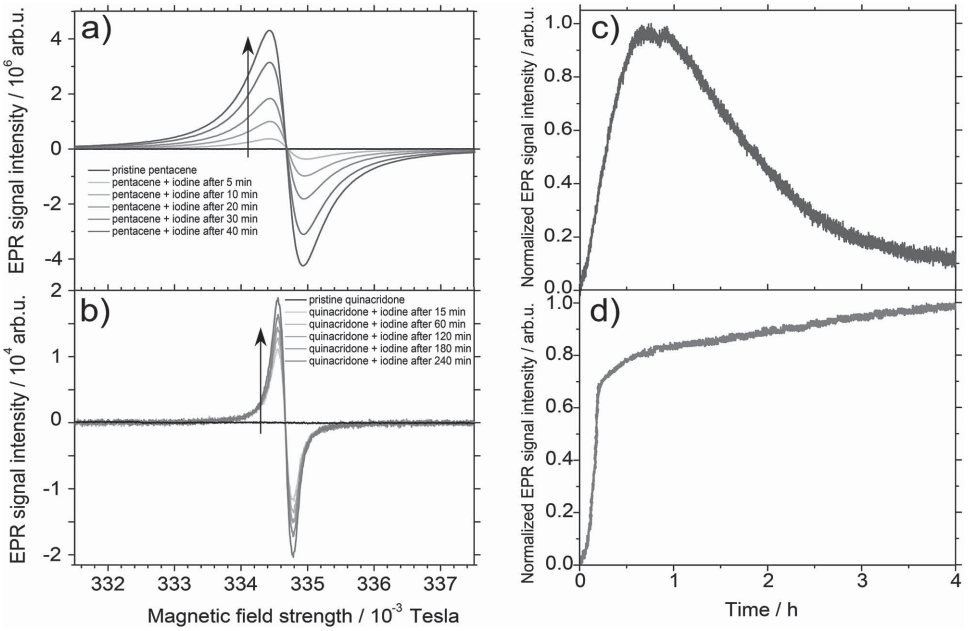

Figure 9. Pristine polycrystalline powder (black line) of a) pentacene and b) quinacridone reveal no EPR signal. After exposure to iodine vapor, clear EPR signals appear, showing that both materials form radical cations. c,d) The EPR signal intensity in a long-term measurement over 4 h for pentacene and quinacridone, respectively. c) After about 40 min of oxidation the EPR signal starts decreasing for pentacene. This behavior is not observed for quinacridone.

In **Figure 9**, the pristine solid form (black curve) of (a) pentacene and (b) quinacridone reveal no detectable EPR signal. Clear EPR signals appear when the oxidation is initiated for both materials. It confirms the radical cation formation as proposed in Figure 2, reactions (1a) and (1b) for pentacene and quinacridone, respectively. Interestingly, for pentacene also reaction (2a) is confirmed. In Figure 9c, the EPR signal intensity decreases after about 40 min in a total 4 h measurement run. This behavior has been reported by Brinkmann et al.[26] as well and it is in agreement with our spectroscopic results. The EPR tracking clearly reveals the disappearing of the radical cation "pentacene$^{+\bullet}$" to its spinless dimer "$(\text{pentacene})^{2+}_2$ ". In contrast, the long-run EPR tracking over 4 h for quinacridone (Figure 9d) corresponds to a persistent radical. These results coincide with the measurements of the spectroscopic part, since we cannot observe differences during the oxidation process. Just one stable species, a radical cation "quinacridone$^{+\bullet}$", is observed in the EPR measurements.

The reorientation of radical cations, say to dimerize, is more likely in pentacene due to weak intermolecular van der Waals forces. Exactly this challenge is prevented by introducing heteroatoms in the molecular frame of pentacene. The resulting rather strong intermolecular hydrogen-bonded crystal lattice in quinacridone leads to chemical stable radical cations confirmed with in situ EPR and spectroscopic measurements.

Summarizing up, dimerization in quinacridone is prevented due to the hydrogen bonds which have a length of about 2 Å and prevent the neighboring molecules from further reactions.[17] In pentacene the situation is different. Since pentacene has no intermolecular hydrogen bonds, intermolecular forces are weaker and pentacene molecules may obviously come close together.

3. Conclusion

Chemical stability represents a severe challenge in various common organic molecular systems. In this work, we elucidate an important aspect, namely, the stability of the doped radical species. Commonly used pentacene does not only suffer from oxidative decomposition by oxygen and moisture, also its radical form is prone to dimerize by itself irreversibly. In this work, we outline the beneficial role of introducing secondary amines and carbonyl groups leading to hydrogen bonds in the solid state on a pentacene frame, as an example. Thus, the desired chemical stability and reversibility for quinacridone is achieved by the functionalization which are preventing not only the molecule against oxygen and moisture but also—most important—leading into a stable and reversible radical form. The heteroatoms protect the organic semiconductors from self-degradation such as dimerization and cyclo-additions. Together with their comparable electronic device performances this enhanced chemical stability offers potential advantages for manifold optoelectronic and bio-related applications.

4. Experimental Section

Sample Preparation: Pentacene was purchased from Sigma-Aldrich and purified twice by temperature gradient sublimation. Quinacridone was purchased from TCI and purified in the same way. These organic semiconductors were evaporated (about 80–100 nm) on the respective substrate. Iodine (Merck) was used directly as received without further purification. Glass slides (0.5 cm × 6 cm for UV–vis measurements and 1 cm × 1 cm for conductivity measurements, respectively) were treated with acetone, isopropyl alcohol, and deionized water as a cleaning

procedure, before further use. Each step was done in an ultrasonic bath for 15 min.

Computational Details: In order to calculate frontier orbitals for both semiconductors, the Gaussian 09 program was used where DFT calculations were done using B3LYP and 6-311+G(d,p) as basis set.[30]

Conductivity Measurements: The conductivities of pentacene and quinacridone were measured in a van der Pauw sample geometry. The organic semiconductors were deposited on glass, as mentioned above, through a specially designed cloverleaf shadow mask. The edge-to-edge distances of the central square were 100 µm by all sides. The cloverleaf was contacted by gold electrodes (about 100 nm) at each leaf using a complementary shadow mask. The final structure is depicted in the inset of Figure 3. The conductivity measurements were performed using a sealed box containing iodine under ambient conditions at room temperature. The resistance was recorded using a LakeShore 8400 HMS system. The four-wire resistance was averaged for all geometries yielding a geometry factor between 0.99 and 1 (ideal). The measurement was started by depositing an iodine crystal adjacent to the sample and repeated every second minute for 30 repeats and finally plotted as function of time.

Raman and IR Measurements: An FT–Raman Bruker MultiRam spectrometer with a liquid N_2 cooled Ge detector and an Nd:YAG laser at 1064 nm was used to record the Raman spectrum of pentacene and quinacridone, respectively. These measurements were done in the powder form. IR experiments were performed using a Bruker FTIR spectrophotometer IFS 66/S with a liquid N_2 cooled mercury–cadmium telluride (MCT) detector working in the attenuated total reflection (ATR) mode. A single-pass parallelepiped ATR crystal in ZnSe was used as a reflection element which was precleaned by polishing with (1 and 0.25 µm) diamond paste and rinsed with acetone in a reflux system before measurements. Pentacene and quinacridone were evaporated onto the ZnSe crystal, as mentioned above.

In situ IR experiments were performed on the same spectrometer using the ATR mode. Pentacene and quinacridone were evaporated onto the ZnSe crystal, as mentioned above. After measuring the spectrum of the neutral form of pentacene and quinacridone, respectively (T_{ref}), the chemical reaction was performed by using iodine as oxidation agent, which was dropped inside a cell to react with the semiconductor (T_{dop}). The difference spectra were calculated as –log (T_{dop}/T_{ref}). For the reversibility measurements, a big iodine crystal was taken, which does not drop inside the iodine tunnel and thus can be removed for the de-doping process. For more details refer to the Supporting Information. A schematic sketch of the chemical cell is shown in Figure 8e.

UV–Vis Measurements: For UV–vis measurements, a Perkin Elmer UV/vis/NIR spectrometer Lambda 1050 with two different detectors, a photomultiplier (PMT) for 175–860 nm, and a cooled InGaAs for 860–1800 nm were used. For the in situ oxidation procedure, the evaporated semiconductors on glass, as described earlier, were fixed in a cuvette and the reference spectrum was measured in absorbance. After that the sample was exposed to iodine vapor over a certain time and further absorbance spectra were measured. Figure 7c shows a schematic sketch of the cell for chemical oxidation in the UV–vis.

EPR Measurements: EPR spectra were recorded at room temperature on Bruker EMX X-band spectrometer (9.45 GHz) with a rectangular TE_{102} cavity and Oxford EPR 910 continuous flow He cryostat operating between 4 and 300 K. Purified polycrystalline powder samples of pentacene and quinacridone, respectively, were placed into 4 mm o.d. high-purity quartz EPR tubes and sealed with a teflon cap under ambient conditions. The spectra of pristine compounds and iodine were recorded one by one revealing no background signal. After that a small piece of iodine was dropped into the EPR tube placed in the EPR cavity containing either pentacene or quinacridone. The signals were measured immediately after iodine was dropped into the tube and then again and again for the period of about 4 h for pentacene and quinacridone, respectively.

Supporting Information

Supporting Information is available from the Wiley Online Library or from the author.

Acknowledgements

Financial support by the Austrian Science Foundation (FWF) within the Wittgenstein Prize scheme for Prof. Sariciftci (FWF [Z 222-N19] Solare Energieumwandlung) and Indigo Circuits (FWF [TRP 294-N19]) as well as the FFG project Flex!PV is gratefully acknowledged.

Received: August 4, 2015
Revised: August 21, 2015
Published online: October 6, 2015

[1] S. R. Forrest, *Nature* **2004**, *428*, 911.
[2] X. Zhang, P. Bäuerle, T. Aida, P. Skabara, C. Kagan, "Organic electronics for a better tomorrow: Innovation, accessibility, sustainability,"http://www.rsc.org/globalassets/04-campaigning-outreach/realising-potential-of-scientists/research-policy/global-challenges/organic-electronics-for-a-better-tomorrow1.pdf(accessed: January 2015).
[3] M. Irimia-Vladu, E. D. Glowacki, G. Voss, S. Bauer, N. S. Sariciftci, *Mater. Today* **2012**, *15*, 340.
[4] Y. Sun, G. C. Welch, W. L. Leong, C. J. Takacs, G. C. Bazan, A. J. Heeger, *Nat. Mater.* **2012**, *11*, 44.
[5] A. Mishra, P. Bäuerle, *Angew. Chem., Int. Ed.* **2012**, *51*, 2020.
[6] D. J. Gundlach, Y. Y. Lin, T. N. Jackson, S. F. Nelson, D. G. Schlom, *IEEE Electron Device Lett.* **1997**, *18*, 87.
[7] Y. Y. Lin, D. J. Gundlach, S. F. Nelson, T. N. Jackson, *IEEE Electron Device Lett.* **1997**, *18*, 606.
[8] M. M. Payne, S. R. Parkin, J. E. Anthony, C.-C. Kuo, T. N. Jackson, *J. Am. Chem. Soc.* **2005**, *127*, 4986.
[9] B. Nickel, M. Fiebig, S. Schiefer, M. Göllner, M. Huth, C. Erlen, P. Lugli, *Phys. Status Solidi A* **2008**, *205*, 526.
[10] H. Klauk, M. Halik, U. Zschieschang, G. Schmid, W. Radlik, W. Weber, *J. Appl. Phys.* **2002**, *92*, 5259.
[11] E. D. Glowacki, M. Irimia-Vladu, M. Kaltenbrunner, J. Gasiorowski, M. S. White, U. Monkowius, G. Romanazzi, G. P. Suranna, P. Mastrorilli, T. Sekitani, S. Bauer, T. Someya, L. Torsi, N. S. Sariciftci, *Adv. Mater.* **2013**, *25*, 1563.
[12] W. Herbst, K. Hunger, *Industrielle Organische Pigmente: Herstellung, Eigenschaften, Anwendung*, Wiley-VCH, Weinheim, Germany **1995**.
[13] R. A. Charvat, *Coloring of Plastics: Fundamentals*, Wiley, Hoboken, NJ, USA **2004**.
[14] D. Berg, C. Nielinger, W. Mader, M. Sokolowski, *Synth. Met.* **2009**, *159*, 2599.
[15] H. Yanagisawa, J. Mizuguchi, S. Aramaki, Y. Sakai, *Jpn. J. Appl. Phys.* **2008**, *47*, 4728.
[16] E. D. Glowacki, L. Leonat, M. Irimia-Vladu, R. Schwödiauer, M. Ullah, H. Sitter, S. Bauer, N. S. Sariciftci, *Appl. Phys. Lett.* **2012**, *101*, 023305.
[17] E. D. Glowacki, M. Irimia-Vladu, S. Bauer, N. S. Sariciftci, *J. Mater. Chem. B* **2013**, *1*, 3742.
[18] E. D. Glowacki, G. Romanazzi, C. Yumusak, H. Coskun, U. Monkowius, G. Voss, M. Burian, R. T. Lechner, N. Demitri, G. J. Redhammer, N. Sünger, G. P. Suranna, S. Sariciftci, *Adv. Funct. Mater.* **2015**, *25*, 776.
[19] I. Osaka, M. Akita, T. Koganezawa, K. Takimiya, *Chem. Mater.* **2012**, *24*, 1235.
[20] N. Gospodinova, E. Tomsik, *Prog. Polym. Sci.* **2015**, *43*, 33.
[21] E. D. Glowacki, H. Coskun, M. A. Blood-Forsythe, U. Monkowius, L. Leonat, M. Grzybowski, D. Gryko, M. S. White, A. Aspuru-Guzik, N. S. Sariciftci, *Org. Electron.* **2014**, *15*, 3521.
[22] J. Dhar, D. P. Karothu, S. Patil, *Chem. Commun.* **2015**, *51*, 97.
[23] *High Performance Pigments*, 2nd ed. (Eds: E. B. Faulkner, R. J. Schwartz), Wiley-VCH, Weinheim, Germany **2009**.

[24] M. Cazayous, A. Sacuto, G. Horowitz, P. Lang, A. Zimmers, R. P. S. M. Lobo, *Phys. Rev. B* **2004**, *70*, 081309.
[25] T. Minakata, I. Nagoya, M. Ozaki, *J. Appl. Phys.* **1991**, *69*, 7354.
[26] M. Brinkmann, V. S. Videva, A. Bieber, J. J. Andre, P. Turek, L. Zuppiroli, P. Bugnon, M. Schaer, F. Nuesch, R. Humphry-Baker, *J. Phys. Chem. A* **2004**, *108*, 8170.
[27] T. Minakata, M. Ozaki, *J. Appl. Phys.* **1993**, *73*, 1819.
[28] D. C. Harris, M. D. Bertolucci, *Symmetry and Spectroscopy: An Introduction to Vibrational and Electronic Spectroscopy*, Oxford University Press, New York, NY, USA **1978**.
[29] H. T. Flakus, A. Jarczyk-Jedryka, *J. At., Mol., Opt. Phys.* **2012**, *2012*, 125471.
[30] M. J. Frisch, G. W. Trucks, H. B. Schlegel, G. E. Scuseria, M. A. Robb, J. R. Cheeseman, G. Scalmani, V. Barone, B. Mennucci, G. A. Petersson, H. Nakatsuji, M. Caricato, X. Li, H. P. Hratchian, A. F. Izmaylov, J. Bloino, G. Zheng, J. L. Sonnenberg, M. Hada, M. Ehara, K. Toyota, R. Fukuda, J. Hasegawa, M. Ishida, T. Nakajima, Y. Honda, O. Kitao, H. Nakai, T. Vreven, J. A. Montgomery Jr., J. E. Peralta, F. Ogliaro, M. Bearpark, J. J. Heyd, E. Brothers, K. N. Kudin, V. N. Staroverov, T. Keith, R. Kobayashi, J. Normand, K. Raghavachari, A. Rendell, J. C. Burant, S. S. Iyengar, J. Tomasi, M. Cossi, N. Rega, J. M. Millam, M. Klene, J. E. Knox, J. B. Cross, V. Bakken, C. Adamo, J. Jaramillo, R. Gomperts, R. E. Stratmann, O. Yazyev, A. J. Austin, R. Cammi, C. Pomelli, J. W. Ochterski, R. L. Martin, K. Morokuma, V. G. Zakrzewski, G. A. Voth, P. Salvador, J. J. Dannenberg, S. Dapprich, A. D. Daniels, O. Farkas, J. B. Foresman, J. V. Ortiz, J. Cioslowski, D. J. Fox, *Gaussian 09*, Gaussian, Inc., Wallingford, CT **2010**.
[31] M. Tamres, S. N. Bhat, *J. Phys. Chem.* **1971**, *75*, 1057.
[32] D. Nabok, P. Puschnig, C. Ambrosch-Draxl, O. Werzer, R. Resel, D.-M. Smilgies, *Phys. Rev. B* **2007**, *76*, 235322.
[33] C. Ambrosch-Draxl, D. Nabok, P. Puschnig, C. Meisenbichler, *New J. Phys.* **2009**, *11*, 125010.